Supporting Information

Qiang et al. 10.1073/pnas.1111305109

SI Text

SI Supporting Methods. ***Peptide synthesis and fibril formation.*** D23N-Aβ_{1-40} (DAEFRHDSGY$_{10}$EVHHQKLVFF$_{20}$AENVGS NKGA$_{30}$IIGLMVGGVV$_{40}$) was synthesized and purified as described previously (1). Monomeric D23N-Aβ_{1-40} was prepared by dissolving the lyophilized peptide in dimethyl sulfoxide at 5–8 mM, then diluting to 100 μM in incubation buffer (10 mM sodium phosphate, pH 7.4, 0.01% NaN_3) Parent fibrils were obtained by quiescent incubation at 6 °C for 7 d. TE fibrils were produced by eight cycles of sonication on ice (Branson model S-250A sonifier, 10% duty cycle, lowest power, 10 min) separated by 48 h incubation periods at 6 °C (Fig. S1*A*). Fibrils after eight generations of seeded growth (Figs. S1 *B* and *C*) were prepared as previously described (1), but at 6 °C and with 3 h incubation periods between generations. SFg2 fibrils were prepared as described in the main text.

Development of structural models. Atomic coordinates for an eight-molecule segment of an antiparallel D23N-Aβ_{1-40} fibril were generated by restrained molecular dynamics and simulated annealing within Xplor-NIH (2). Only residues 15–40 were included. Potential energy functions included potentials representing distance restraints derived from 2D RAD spectra, 2D CHHC spectra, PITHIRDS-CT data, and REDOR data (see Table S2), and backbone dihedral angle restraints derived from ^{13}C chemical shifts (see Table S1). Standard bond length, bond angle, improper dihedral, and nonbonded repulsive potentials were also used.

For structures shown in Fig. 4 and Fig. S6, artificial uniaxial "residual dipolar coupling" (RDC) restraints for backbone N-H bond vectors in residues 17–21 and 31–35 were also included. RDCs were not measured experimentally, of course, but the RDC potential term in Xplor-NIH provides a simple means of restraining N-H bond directions in β-strand segments to be approximately parallel to an external axis (which then becomes the long fibril axis), as they should be in any cross-β structure. The RDC potential does not prevent the cross-β structure from developing a gradual twist about the fibril axis, as commonly observed in electron microscopy studies of amyloid fibrils (3–5). To produce the desired alignment of N-H bonds, the artificial RDC values for residues 17–21 and 31–35 were set equal to twice the anisotropy (D_a) of the alignment tensor.

Interstrand O-H_N and O-C distance restraints were used to represent interstrand hydrogen-bonding patterns identified from the 2D CHHC spectra. These distance restraints were assigned to pairs of D23N-Aβ_{1-40} molecules in a way that is consistent with an antiparallel β-sheet. For example, for odd j, O-H_N restraints were applied between O of I31 in molecule j and H_N of M35 in molecule $j+1$, and between O of I32 in molecule $j+1$ and H_N of L34 in molecule $j+2$; for even j, O-H_N restraints were applied between O of I31 in molecule j and H_N of M35 in molecule $j-1$, and between O of I32 in molecule $j-1$ and H_N of L34 in molecule $j-2$.

Xplor-NIH runs began with eight copies of the peptide in an extended conformation, placed far apart from one another (40 Å center-of-mass spacings) with antiparallel alignments. A brief period of high-temperature dynamics (3,000 K, 5,000 simulation steps) was performed, including dihedral angle potentials (scaling factor equal to 5), but not including distance potentials or RDC potentials. Annealing was then carried out in two stages. In the first stage (3,000 K to 500 K, 5×10^6 total steps), distance and dihedral angle potentials were applied, but not RDC potentials. The scaling factor for distance potentials was ramped from 1 to 20. The scaling factor for dihedral angle potentials was set to 20. In the second stage (500 K to 10 K, 3.9×10^6 total steps), the scaling factor for dihedral angle potentials was set to 20 and the scaling factor for distance potentials was ramped from 20 to 200. RDC potentials were applied, with a scaling factor that was ramped from 1 to 5. Energy minimization was performed after the second annealing stage. Forty Xplor-NIH runs were performed, yielding three structures with no violations of the distance restraints (0.5 Å threshold). The lowest-energy structure was then selected as the initial condition for a second iteration of the two-stage annealing protocol. Simulation conditions were as described above, but high-temperature dynamics were performed at 1,500 K, the first annealing stage proceeded from 1,500 K to 500 K in 1.0×10^6 steps, and the second annealing stage proceeded from 500 K to 10 K in 7.8×10^5 steps. Forty Xplor-NIH runs were performed. The ten structures with lowest restraint energies were retained as the final structures and deposited in the Protein Data Bank as PDB file 2LNQ. Fig. S6 shows superpositions of the ten final structures. Root-mean-squared deviations (rmsd) from the mean of the ten structures are 0.86 Å for backbone atoms and 1.50 Å for non-hydrogen atoms in residues 16–34 of the central pair of molecules. The lowest-energy structure is displayed in Fig. 4. Total target energies range from 136.53 to 137.89, in Xplor-NIH units. No violations of bond angles, bond lengths, improper angles, or RDC restraints occur in the final structures (thresholds of 5°, 0.05 Å, 5°, and 0.5 Hz, respectively). No violations of distance restraints occur (0.5 Å threshold beyond the limits in Table S2; 240 total restraints). An average of 20.8 ± 2.4 nonbonded distance (i.e., van der Waals contacts) violations occur (0.2 Å threshold), with the largest violation being 0.39 Å. An average of 15.0 ± 1.6 violations of dihedral angle restraints occur (5° threshold beyond the TALOS+limits; 280 total restraints), with the rms violation being $2.13° \pm 0.039°$ and the largest violation being 8.5°.

Inclusion of artificial RDC restraints as described above has the effect of reducing the rmsd values in the final structures, but otherwise does not affect the structures qualitatively. When structures are calculated with the same protocol, but without RDC restraints, the rmsd for residues 16–34 in the central pair of molecules is 0.94 Å for backbone atoms and 1.58 Å for non-hydrogen atoms (including the 10 lowest-energy structures from 40 Xplor-NIH runs). Rmsd values between the lowest-energy structure calculated with RDC restraints and the 10 lowest-energy structures calculated without RDC restraints are 0.98 Å for backbone atoms and 1.62 Å for non-hydrogen atoms.

Cytotoxicity measurements. Cultures of dissociated hippocampal neurons were prepared from embryonic day 18 Sprague Dawley (Harlan Sprague Dawley) rats as previously described (6). Briefly, hippocampal cells were mechanically dissociated by trituration following 0.05% trypsin-EDTA (Invitrogen) treatment and were seeded into polyethyleneimine-coated 35 mm dishes at a density of 10,000 cells/cm^2. The culture medium consisted of Eagle's minimum essential medium containing 10 mM sodium bicarbonate, 1% glucose, 1 mM L-glutamine, 20 mM KCl, 1 mM sodium pyruvate, and 10% (v/v) heat-inactivated fetal bovine serum (Sigma). After a 4–6 h period to allow cell attachment to the substrate, the culture medium was replaced with Neurobasal medium (Life Technologies) containing B27 supplements (Invitrogen) in a humidified atmosphere (6% CO_2/94% room air) at 37 °C. Experiments were performed on cells that had been in culture for 7 d. Prior to addition to cell cultures, D23N-Aβ_{1-40}

and WT-Aβ_{1-40} fibril solutions were dialyzed against 10 mM phosphate buffer for 2 d to remove residual DMSO and NaN_3, then pelleted at 435,000 × *g* for 2 h. The pellet was resuspended in Neurobasal medium without B27 and sonicated for several minutes in a water bath sonicator, until solutions became fully transparent. Solutions were prepared with fibrillized peptide concentrations of 1, 5, 10 and 30 μM and applied to the culture dishes (immediately after removing the existing culture medium from each dish). Viable neurons in optical microscope images of marked areas of the dishes were counted before exposure to fibrils and after 24 h and 48 h exposure periods. Ratios of these counts were used as measures of neuronal survival. The culture medium was not changed before recording images. Fibrils are not directly visible in the images in Fig. S7*A* because their dimensions are below the optical resolution limit. No dye or stain was applied to the culture dishes.

1. Qiang W, Yau WM, Tycko R (2011) Structural evolution of Iowa mutant β-amyloid fibrils from polymorphic to homogeneous states under repeated seeded growth. *J Am Chem Soc* 133:4018–4029.
2. Schwieters CD, Kuszewski JJ, Clore GM (2006) Using Xplor-NIH for NMR molecular structure determination. *Prog Nucl Magn Reson Spectrosc* 48:47–62.
3. Antzutkin ON, Leapman RD, Balbach JJ, Tycko R (2002) Supramolecular structural constraints on Alzheimer's β-amyloid fibrils from electron microscopy and solid state nuclear magnetic resonance. *Biochemistry* 41:15436–15450.
4. Goldsbury CS, Wirtz S, Muller SA, Sunderji S, Wicki P, Aebi U, Frey P (2000) Studies on the in vitro assembly of Aβ_{1-40}: Implications for the search for Aβ fibril formation inhibitors. *J Struct Biol* 130:217–231.
5. Paravastu AK, Leapman RD, Yau WM, Tycko R (2008) Molecular structural basis for polymorphism in Alzheimer's β-amyloid fibrils. *Proc Natl Acad Sci USA* 105:18349–18354.
6. Mattson MP, Cheng B, Davis D, Bryant K, Lieberburg I, Rydel RE (1992) β-Amyloid peptides destabilize calcium homeostasis and render human cortical neurons vulnerable to excitotoxicity. *J Neurosci* 12:376–389.
7. Paravastu AK, Qahwash I, Leapman RD, Meredith SC, Tycko R (2009) Seeded growth of β-amyloid fibrils from Alzheimer's brain-derived fibrils produces a distinct fibril structure. *Proc Natl Acad Sci USA* 106:7443–7448.

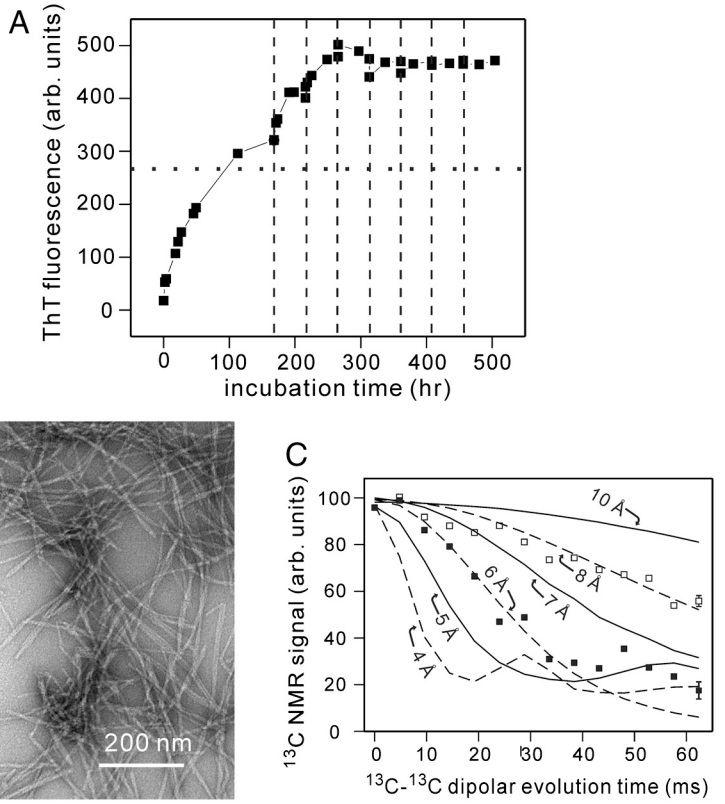

Fig. S1. (*A*) Thioflavin T (ThT) fluorescence measurements during the preparation of TE fibrils. Fluorescence was excited at 423 nm and detected at 490 nm, using 9 μM D23N-Aβ_{1-40} and 36 μM ThT. After the initial 160 h incubation period, the sample was sonicated for 10 min at times indicated by vertical dashed lines. Intermittent sonication kept the fibrils short, accelerating the approach to thermodynamic equilibrium by increasing the concentration of fibril ends to and from which D23N-Aβ_{1-40} could associate and dissociate. The asymptotic fluorescence intensity of approximately 460 units for TE fibrils was significantly higher than the intensity for parent fibrils (approximately 320 units). Horizontal dotted line indicates the ThT fluorescence intensity for SFg2 fibrils (approximately 270 units). (*B*) TEM image of negatively stained D23N-Aβ_{1-40} fibrils after 8 generations of seeded growth at 6 °C and pH 7.4, starting with parent fibrils. (*C*) PITHIRDS-CT data for parent fibrils (open squares) and fibrils produced by eight generations of seeded growth (solid squares). Fibrils were ^{13}C-labeled at methyl carbons of A21 residues. Dashed and solid curves are simulated PITHIRDS-CT data for linear chains of ^{13}C nuclei with the indicated spacings.

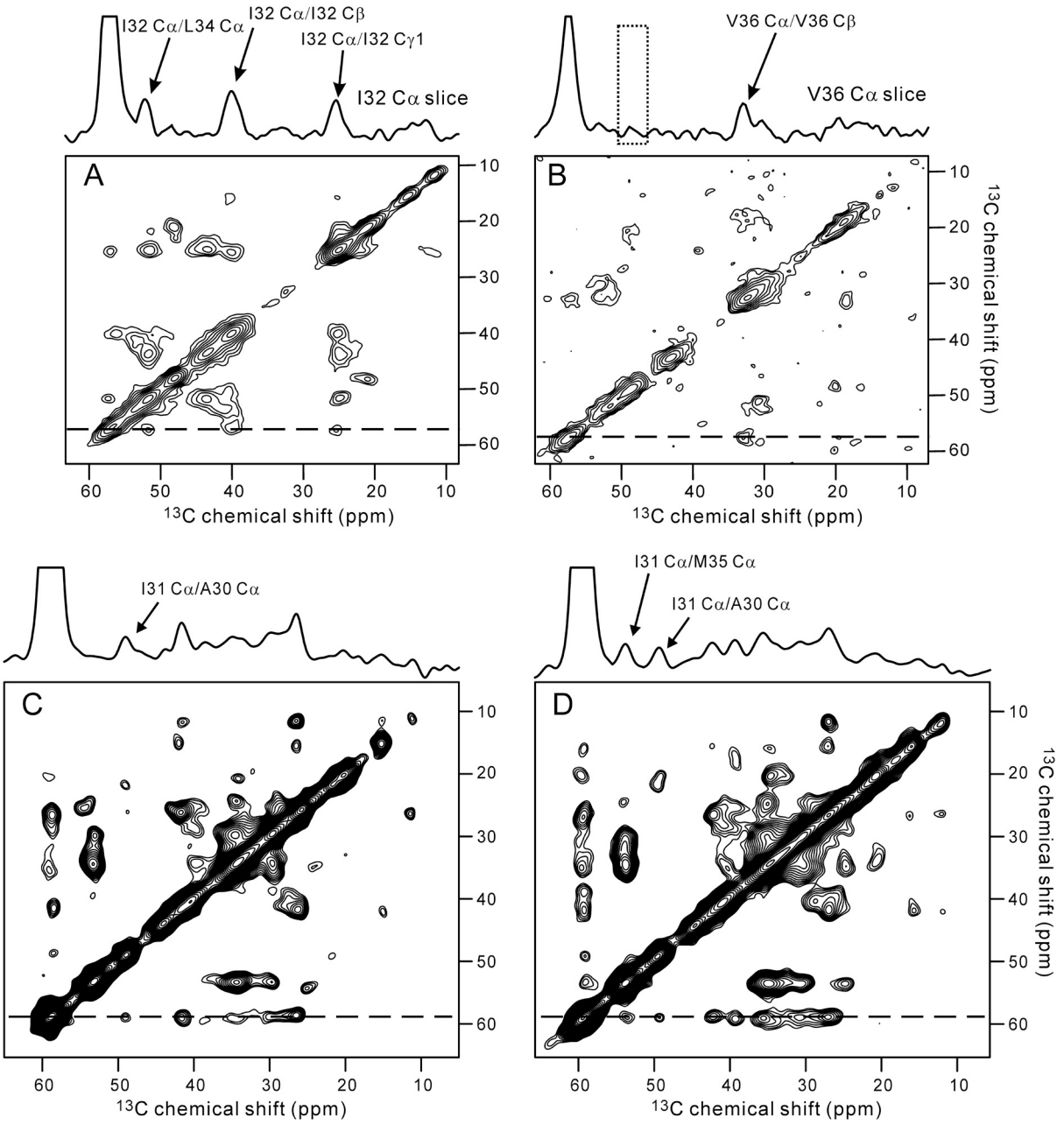

Fig. S2. 2D CHHC spectra of SFg2 fibril samples. (*A*,*B*) Spectra of samples *C* and *D*, respectively, with 1D slices at $^{13}C_{\alpha}$ chemical shifts of I32 and V36 (dashed lines). Strong I32 C_{α}/L34 C_{α} crosspeaks indicate antiparallel β-sheets with $31 + k \leftrightarrow 35 - k$ registry, consistent with Fig. 3*A*. The absence of a detectable A30 C_{α}/V36 C_{α} crosspeak in the dotted rectangle in panel B indicates that A30 and V36 define the edges of the C-terminal β-sheet in SFg2 fibrils. These spectra were obtained at 9.39 T and 20.00 kHz MAS frequency. (*C*) Spectrum of a sample in which peptide A (uniformly ^{15}N,^{13}C-labeled at K16, E22, A30, I31, M35, G38, and V39) was diluted in unlabeled D23N-Aβ_{1-40}, with a 1:2 molar ratio. This spectrum was obtained at 14.1 T and 20.00 kHz MAS frequency. (*D*) Spectrum of undiluted sample A, obtained at 14.1 T and 20.00 kHz MAS frequency. The strong I31 C_{α}/M35 C_{α} crosspeaks observed in this spectrum are suppressed in the spectrum of the diluted sample, as expected if the crosspeak arises from intermolecular ^{13}C polarization transfers.

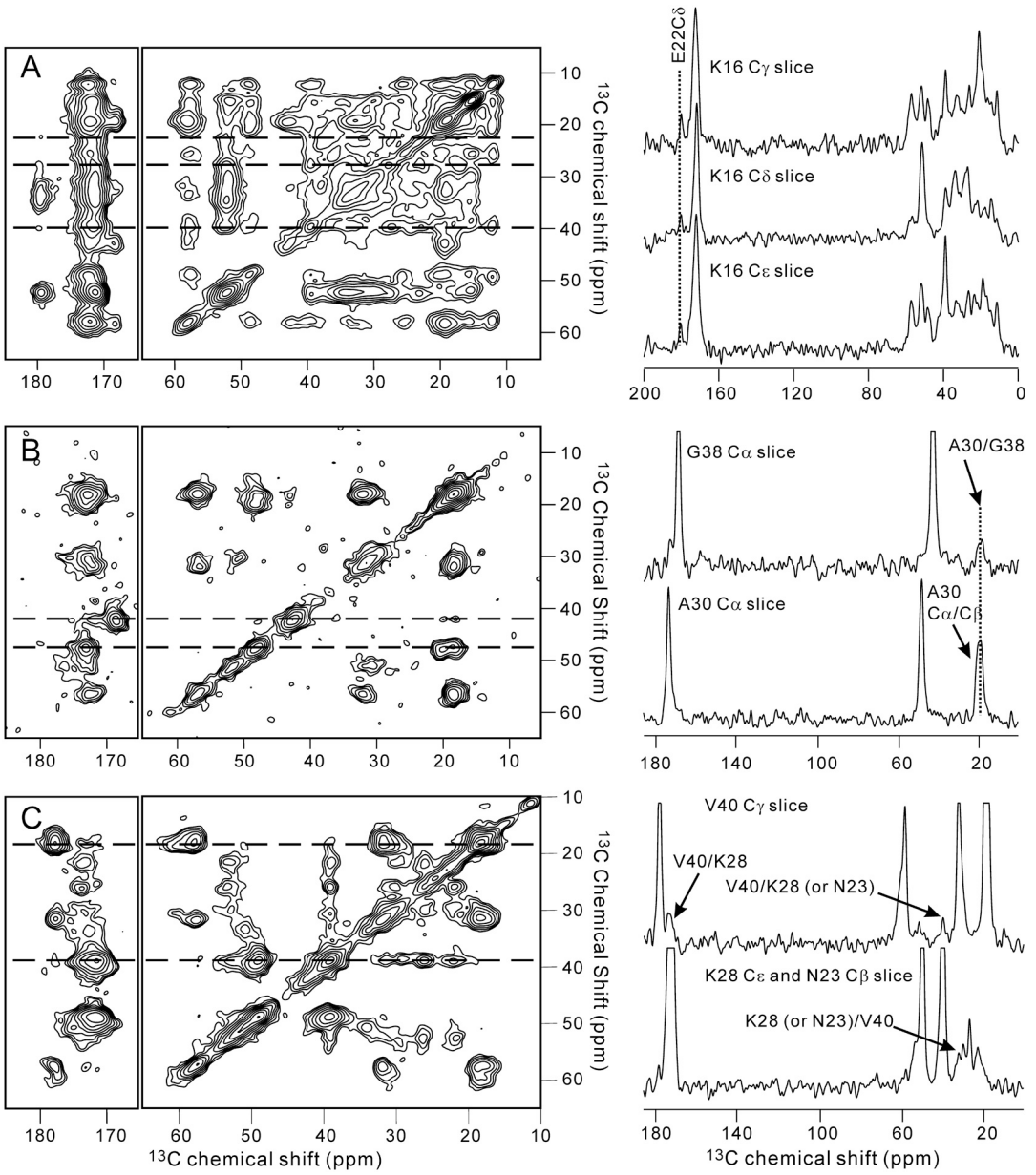

Fig. S3. 2D RAD spectra of SFg2 fibrils samples *A*, *D* and *E* (*A*, *B*, and *C*, respectively). 1D slices at ^{13}C chemical shifts indicated by dashed lines show K16/E22, G38/A30, and K28/V40 crosspeaks.

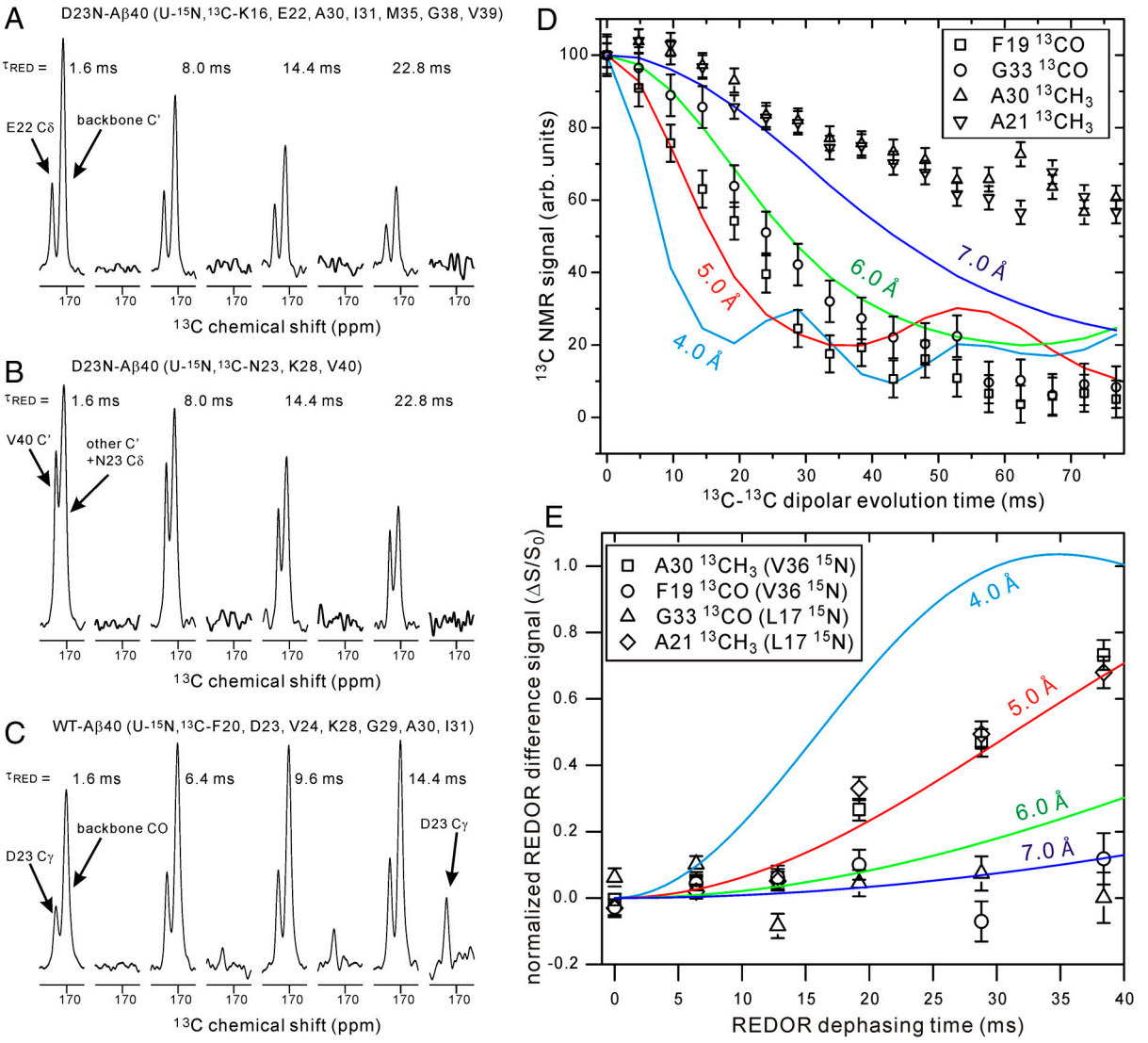

Fig. S4. Additional structural measurements on SFg2 fibril samples. (*A*,*B*) Frequency-selective REDOR measurements on samples *A* and *E* to test for the presence of K16-E22 and K28-V40 salt bridge interactions. At each value of the REDOR dephasing time τ_{RED}, carbonyl regions of the S_0 and ΔS spectra are shown, where S_0 is the undephased ^{13}C NMR signal and ΔS is the difference between undephased and dephased signals. Absence of a detectable ΔS signal for E22 C_δ and V40 C′ sites indicates that distances from these sites to side-chain amino ^{15}N sites of K16 and K28, respectively, exceed 4.5 Å. (*C*) Frequency-selective REDOR measurements on WT-Aβ_{1-40} fibrils that contain D23-K28 salt bridges, showing clear ΔS signals for D23 C_γ, with a dependence of $\Delta S/S_0$ on τ_{RED} that indicates ^{15}N-^{13}C distances less than 3.5 Å. (*D*) ^{13}C PITHIRDS-CT measurements on SFg2 samples with ^{13}C labels at the F19 carbonyl and A30 methyl sites and a ^{15}N label at V36 (squares and upward triangles) and with ^{13}C labels at the G33 carbonyl and A21 methyl sites and a ^{15}N label at L17 (circles and downward triangles). Data are corrected for natural-abundance ^{13}C signal contributions (estimated from the sequence in residues 15–40 to be 25% for carbonyl and 19% for methyl data), which are assumed to decay linearly to 70% of their initial values over the 76.8 ms evolution time. Curves are simulated data for linear chains of ^{13}C nuclei with the indicated spacings. Relatively short intermolecular distances for G33 and F19 carbonyls and long distances for A21 and A30 methyls are consistent with $17 + k \leftrightarrow 21 - k$ and $31 + k \leftrightarrow 35 - k$ registry for the two β-strands in SFg2 fibrils, as depicted in Fig. 4. (*E*) ^{13}C-detected ^{15}N-^{13}C REDOR measurements on the same samples as in panel D, showing relatively short distances between A30 methyl and V36 amide sites and between A21 methyl and L17 amide sites, consistent with $17 + k \leftrightarrow 21 - k$ and $31 + k \leftrightarrow 35 - k$ registries . Data are corrected for natural-abundance ^{13}C signal contributions (25% for carbonyl and 19% for methyl data), which are assumed to have no REDOR dephasing. Curves are simulated data for ^{15}N-^{13}C pairs with the indicated internuclear distances. Distances between F19 carbonyl and V36 amide sites and between G33 carbonyl and L17 amide sites are longer, as expected for the SFg2 structure in Fig. 4.

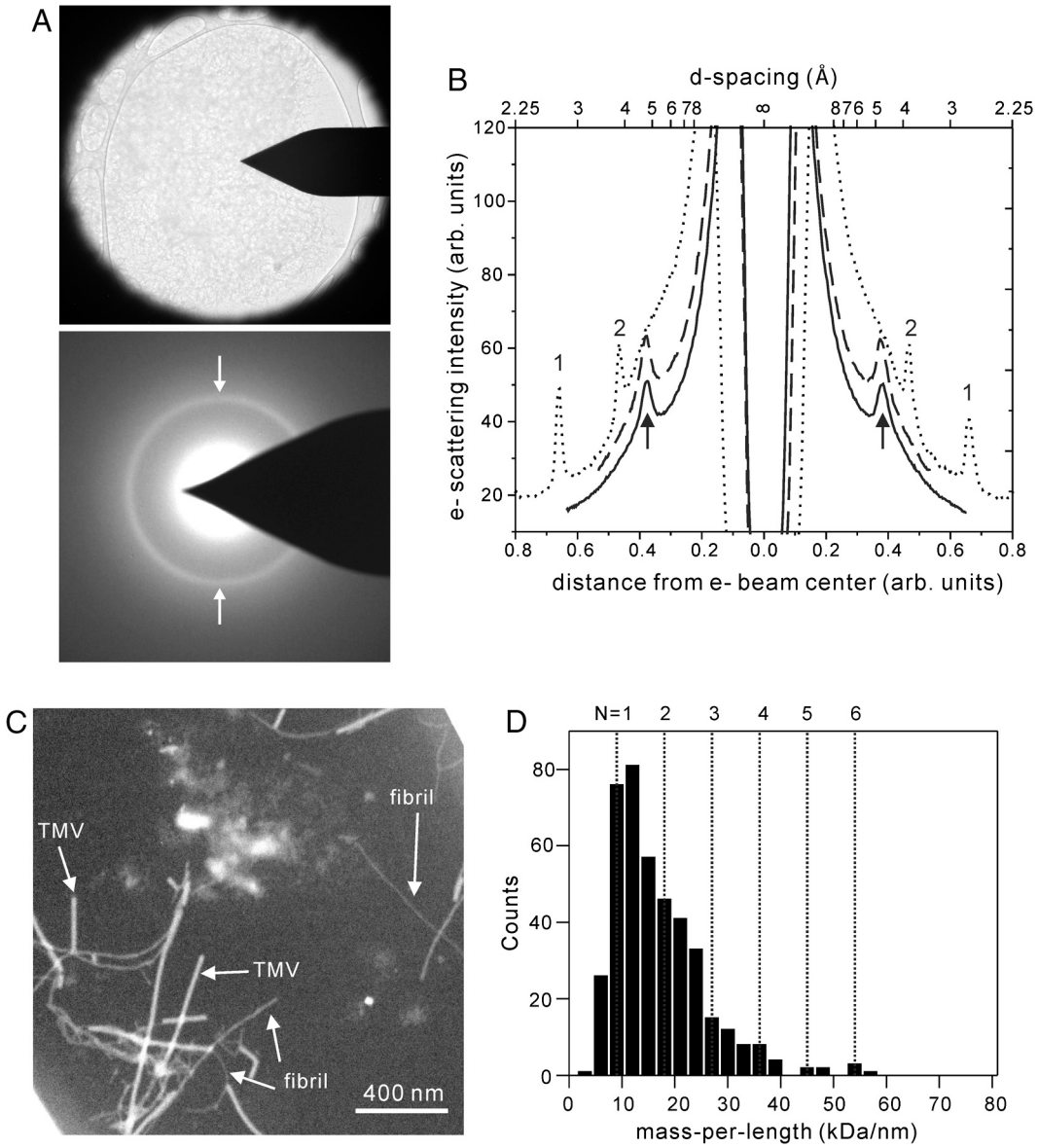

Fig. S5. (*A*) Bright-field image and electron diffraction image (top and bottom, respectively) of unstained SFg2 fibrils on a thin carbon film. White arrows indicate the 4.8 Å diffraction ring. Horizontal lack pointer is the beam stop. (*B*) Electron diffraction patterns from SFg2 fibrils (solid line), which contain antiparallel β-sheets, and D23N-Aβ_{1-40} fibrils prepared by multiple generations of seeded growth as in Fig. S1*B* (dashed line), which contain parallel β-sheets. These patterns are vertical sections through the corresponding diffraction images. Spacings indicated by arrows are 4.77 Å for the antiparallel and 4.79 Å for the parallel structures. Dotted line is diffraction data for thallium chloride crystals, used to calibrate the spacings. Peaks 1 and 2 are 2.72 Å and 3.84 Å. (*C*) Example of a dark-field TEM image of unstained SFg2 fibrils that was used for quantitative mass-per-length (MPL) measurements. Tobacco mosaic virus (TMV) particles were included as image intensity calibration standards. (*D*) MPL histogram constructed from measurements on fibrils in 60 dark-field images. MPL values expected for D23N-Aβ_{1-40} fibrils comprised of N cross-β layers are indicated by vertical dashed lines, for N from 1 to 6.

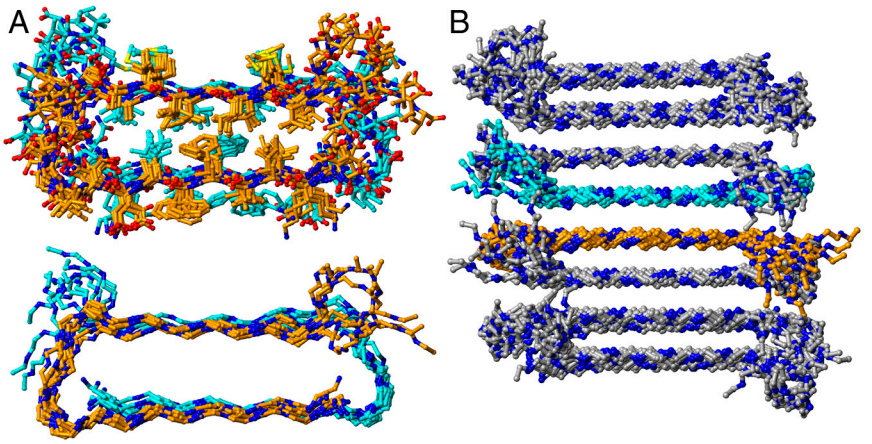

Fig. S6. Superposition of 10 structures for residues 15–40 in antiparallel D23N-Aβ_{1-40} fibrils (PDB file 2LNQ). (*A*) Non-hydrogen atoms (*Top*) and backbone atoms (*Bottom*) of the central pair of molecules in the eight-molecule system. Carbon atoms of the front molecule are orange. Carbon atoms of the back molecule are cyan. The 10 structures are viewed parallel to the fibril axis and aligned to minimize the root-mean-squared deviation of backbone atoms in residues 16–34 of the central pair of molecules. (*B*) Backbone atoms of the entire eight-molecule system, viewed perpendicular to the fibril axis.

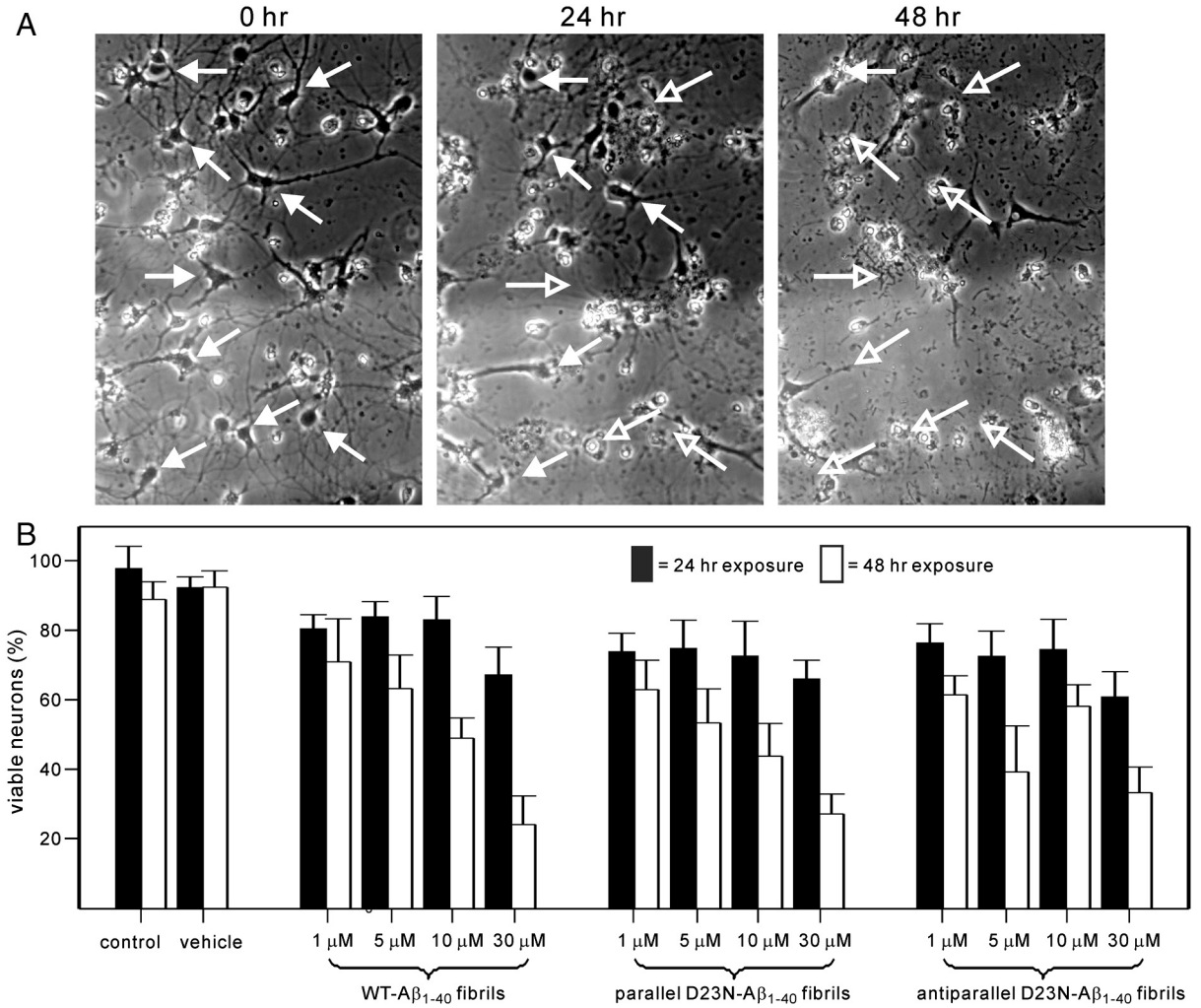

Fig. S7. Neurotoxicity measurements on D23N-Aβ_{1-40} and WT-Aβ_{1-40} fibrils. (*A*) Phase contrast microscope images of primary rat embryonic hippocampal neurons after 0 h, 24 h, and 48 h exposure to SFg2 fibrils at $[\text{D23N-A}\beta_{1-40}] = 10$ μM. Neurons in the same area of the culture dish are shown in each image. Solid-head arrows indicate viable neurons. Hollow-head arrows indicate positions where neurons have died or disappeared. (*B*) Neuronal survival at 24 h (black bars) and 48 h (white bars) for the indicated conditions, measured as the ratio of the number of viable neurons at 24 h or 48 h in designated microscope fields to the number of viable neurons in the same fields at 0 h. Antiparallel D23N-Aβ_{1-40} fibrils are SFg2. Parallel D23N-Aβ_{1-40} fibrils are as in Fig. S2. WT-Aβ_{1-40} fibrils are 2-fold symmetric structures described by Petkova et al. (7) Vehicle measurements are after addition of 20 μL of 50 mM phosphate buffer (without fibrils) to the culture dishes (1 mL total volume of culture medium). Control measurements are without exposure to fibrils or buffer. Error bars indicate standard deviations from nine independent measurements (3 separate regions in 3 separate culture dishes for each condition), with 80–200 neurons at 0 h in each measurement.

Table S1. ^{13}C NMR chemical shifts (relative to tetramethylsilane) in SFg2 D23N-Aβ_{1-40} fibrils and backbone dihedral angles predicted by TALOS+

	chemical shift (ppm)						
Residue	CO	C_α	C_β	C_γ	C_δ	C_ε	predicted φ,ψ (°)*
Q15	171.1	51.3	30.8	32.1	175.2		
K16	170.7	52.7	34.4	22.5	27.3	38.8	−122±16, 130±14
V18	170.2	58.2	32.6	18.8			−132±13, 139±18
F19	170.8	53.1	41.0				−123±17, 133±17
	172.3	49.0	39.2				
F20	169.8	53.0	40.3				−128±13, 134±17
A21	171.8	47.8	20.6				−124±20, 143±15
	172.1	47.6	22.4				
E22	170.7	52.6	34.4	34.4	179.0		−131±14, 140±13
N23	171.0	49.6	39.6	171.0			−109±16, 133±13
K28	173.3	53.5	29.8	21.8	26.1	39.1	
A30	172.6	48.4	20.1				−129±23, 133±12
I31	171.5	57.3	39.0	24.9,14.6	11.5		−126±17, 131±16
I32	171.7	56.4	39.2	25.1,14.9	11.4		−126±16, 130±22
L34	171.2	51.1	43.7	23.9,22.9			−128±16, 132±19
M35	172.3	52.0	33.8	29.4			−122±22, 136±14
V36	171.5	57.5	32.2	18.3			−123±19, 138±20
G38	168.0	42.8					
V39	172.1	58.7	31.2	18.4			−120±34, 142±19
V40	177.2	58.3	31.7	18.1			

*Dihedral angles for L17 ($\phi,\psi = -120 \pm 16°, 130 \pm 14°$) and G33 ($\phi,\psi = -118 \pm 25°, 145 \pm 26°$) were also predicted by TALOS+ and used in Xplor-NIH calculations.

Table S2. Summary of structural restraints used in the development of molecular models for SFg2 D23N-Aβ_{1-40} fibrils

Restraint	Value	Experimental basis
Backbone φ and ψ angles	Values and uncertainties given in Table S1*	TALOS+predictions from ^{13}C NMR chemical shifts
Interstrand backbone hydrogen bonding for the following residue pairs: V18/F20, I31/M35, and I32/L34	1.5–1.7 Å for interstrand O-H_N distances between hydrogen-bonded residues; 2.5–2.7 Å for interstrand O-N distances	Nonsequential C_α/C_α crosspeaks in 2D CHHC spectra
Contacts between the following atom pairs: F19C_ζ/I32C_δ, F19C_ζ/I32$C_{\gamma 2}$, F19C_ζ/L34C_γ, A21C_α/I32C_δ, A21C_β/I32C_δ, I32$C_{\gamma 2}$/L34C_α, I32$C_{\gamma 2}$/L34C_β	3.0–7.0 Å F19/I32 and A21/I32 3.0–9.0 Å for I32/L34 3.0–6.0 Å for F19/L34	Nonsequential interresidue crosspeaks in 2D RAD spectra*
Contacts between the following atom pairs: A30C_β/G38C_α, K28CO/V40$C_{\gamma 1}$, K28C_ε/V40$C_{\gamma 1}$, K28C_ε/V40C_β, K16C_ε/E22C_δ, K16Cγ/E22C_δ, and K16C_δ/E22C_δ	3.0–7.0 Å	Nonsequential interresidue crosspeaks in 2D RAD spectra†
Intermolecular F19-F19 and G33-G33 CO-CO distances between neighboring β-strands	4.5–5.5 Å	PITHIRDS-CT ^{13}C-^{13}C recoupling data
Intermolecular A30Cβ-V36N and A21Cβ-L17N distances between neighboring β-strands	4.9–5.5 Å	REDOR ^{15}N-^{13}C recoupling data
Alignment of backbone N-H bond vectors for residues 17–21 and 31–35 with a single external axis‡	Artificial residual dipolar couplings (see *Supporting Methods*)	Cross-β structure indicated by electron diffraction

*Treated as intramolecular contacts for simplicity, although the 2D RAD data do not directly distinguish intramolecular side chain–side chain contacts from contacts between side chains of neighboring molecules within a β-sheet.

†Treated as intermolecular because intramolecular contacts between these atom pairs would be inconsistent with the β-strand conformations of residues 16–22 and 30–36.

‡Chosen for their β-strand conformation and involvement in antiparallel interstrand hydrogen bonds.